ACS Photonics

pubs.acs.org/journal/apchd5

Article

Phenotypic Analysis of Microalgae Populations Using Label-Free Imaging Flow Cytometry and Deep Learning

Çağatay Işıl,[†] Kevin de Haan,[†] Zoltán Göröcs,[†] Hatice Ceylan Koydemir,[†] Spencer Peterman, David Baum, Fang Song, Thamira Skandakumar, Esin Gumustekin, and Aydogan Ozcan*

Cite This: https://dx.doi.org/10.1021/acsphotonics.1c00220

Read Online

ACCESS | Metrics & More | Article Recommendations | Supporting Information

ABSTRACT: Environmental factors such as temperature, nutrients, and pollutants affect the growth rates and physical characteristics of microalgae populations. As algae play a vital role in marine ecosystems, the monitoring of algae is important to observe the state of an ecosystem. However, analyzing these microalgae populations using conventional light microscopy is time-consuming and requires experts to both identify and count the algal cells, which in turn considerably limits the volume of the samples that can be measured in each experiment. In this work we use a high-throughput and field-portable imaging flow cytometer to perform automated label-free phenotypic analysis of marine microalgae populations using image processing and deep learning. The imaging flow cytometer provides color intensity and phase images of microalgae contained in a liquid sample by capturing and reconstructing the lens-free color holograms of the continuously flowing liquid at a flow rate of 100 mL/h. We extracted the spatial and spectral features of each algal cell in a sample from these holographic images and performed automated algae identification using convolutional neural networks. These features, alongside the composition and growth rate of the algae within the samples, were analyzed to understand the interactions between different algae populations as well as the effects of toxin exposure. As proof of concept, we demonstrated the effectiveness of the system by analyzing the impact of various concentrations of copper on microalgae monocultures and mixtures.

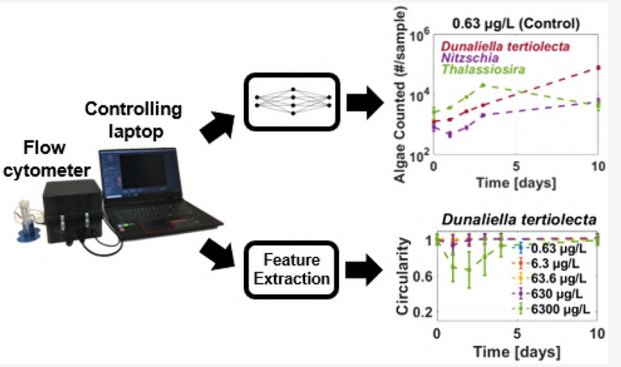

KEYWORDS: *imaging flow cytometry, microalgae, deep learning, phenotypic analysis*

Microalgae are vital to ecosystems around the world, as they provide approximately half of the primary production of our planet and form the basis of the oceanic food chain.[1] Various environmental factors such as high or low temperature, deficiency of nutrients, and pollutants (e.g., heavy metals and nano/micro plastics) affect the growth pattern and overall health of these organisms. Exposure to toxic compounds not only harm microalgae populations, but also their effects propagate through the food web affecting higher-level organisms such as zooplankton, invertebrates, fish, aquatic mammals and birds, and humans. Through the process of bioaccumulation, pollutants build up in algal tissues over time as algae absorb them from the aquatic environment. This in turn affects the higher-level organisms through biomagnification, which occurs as the contaminated algae are consumed and the pollutants become more heavily concentrated in the consumers' tissue with increased severity at higher levels in the food chain.[2]

There is large variability between species in their response and tolerance to different pollutants,[3] and the effect of these pollutants on microalgae is not fully explored and is continuously being studied. One of the main types of pollutants occurring in marine environments is heavy metals such as copper, mercury, and lead.[4] They induce oxidative stress in microalgae by preventing the inactivation of reactive oxygen species, which can damage tissues.[3] While copper is important for algal metabolism as it serves an essential role as a redox cofactor for enzymes, it can become toxic at higher concentrations. Copper compounds can easily enter aquatic ecosystems through surface runoff from urban sources such as automobile brake emissions, sidings, and roofs,[5] as well as copper mining.[6] In these ecosystems, the effects of copper can be highly dependent on the types of algae affected; different species demonstrate highly varying levels of sensitivity to copper with tolerance levels ranging over 3 orders of magnitude[7] in concentration.

Received: February 8, 2021

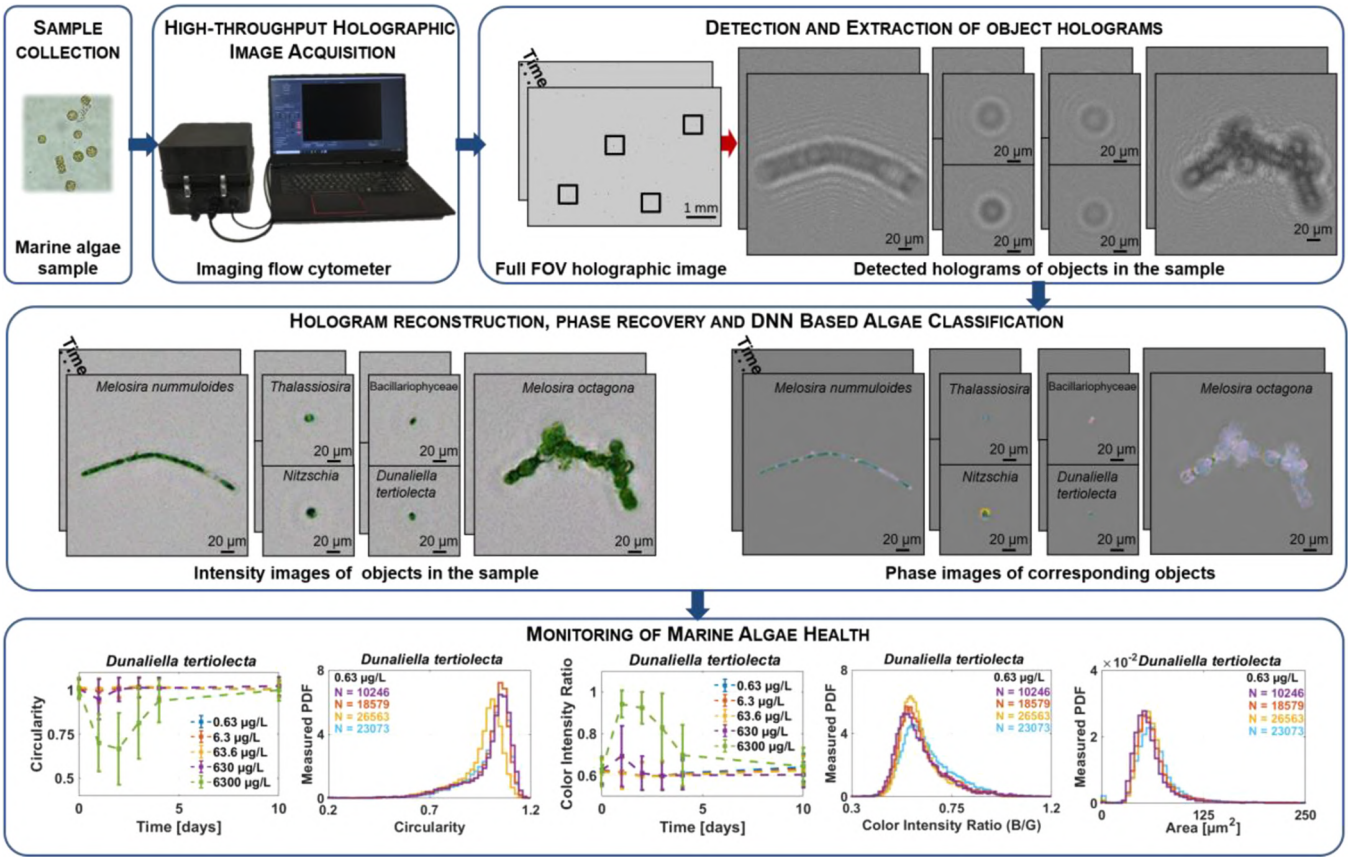

Figure 1. Overview of holographic imaging flow cytometry system and the processing workflow used for monitoring algae populations. The algae sample can be automatically analyzed by the imaging flow cytometer without the need for sample preparation or external labeling. The device captures in-line holograms of the contents of continuously flowing water samples at a throughput of 100 mL/h. Each frame has a field-of-view of 30 mm^2 and contains the holograms of the flowing objects. These acquired holograms of individual objects are automatically detected, extracted, and reconstructed to provide the phase and intensity images of the detected objects at red, green, and blue illumination channels. Convolutional neural networks and traditional feature extraction algorithms are then used to automatically analyze and quantify the composition of the algae samples.

A variety of studies have been used to analyze the effects of copper on algae biodiversity.[7−9] For example, a study by Gustavson et al. found that species richness and dominance in microalgal enclosures fell in response to increased copper exposure, while species evenness rose.[8] By analyzing uptake and internalization of copper, growth rate inhibition has been related not only to copper uptake rates, but also to cell detoxification characteristics of microalgae.[9] Moreover, two algae species, that is, *Dunaliella tertiolecta* (*D. tertiolecta*) and *Minutocellus polymorphus* have been stated as one of the most copper-tolerant and copper-sensitive microalgae species, respectively.[7] As copper is usually used in pesticide formulation, its ecotoxicological effects upon microalgae have been investigated, and the critical side effects of pesticides for the entire food web have also been reported.[10] Furthermore, it has been shown that communities of algae can develop pollution-induced community tolerance (PICT) if exposed to contaminants such as copper.[8] According to PICT, pollutants remove species that are sensitive to them; therefore, exerting a selective pressure that induces the ecological community to take on a new structure that has a higher tolerance of the pollutant.[8] It was also shown that various algae species can change their metabolism to become more tolerant to contaminants.[11]

Microalgae form a particularly rich source of information about the long-term effects of pollution on biodiversity in the marine environment due to their short generation times and high sensitivity to changing environmental conditions.[12] However, studying the effects of pollutants on algae is challenging due to the labor-intensive nature of repeatedly sampling, imaging, and counting the various species in a mixture over time. To analyze these effects on algae, high-throughput imaging flow cytometry can be used to automatically image individual microalgae in a liquid sample.[13] Existing imaging flow cytometer systems such as CytoSense[14] (Cytobouy b.v.), Flowcam[15] (Fluid Imaging Technologies), and Imaging Flowcytobot[16] (McLane Research Laboratories) are relatively expensive (costing ∼$40000−100000), bulky and heavy (9−30 kg), partially limiting their accessibility to researchers. Furthermore, most of them are not portable enough for field use, which can limit the types of studies that can be performed.

Recently, we have developed a lightweight, high-throughput, and field-portable imaging flow cytometer system.[17,18] This label-free imaging cytometer (shown in Figures 1 and S1) has the dimensions of 19 cm × 19 cm × 16 cm, weighs 1.6 kg, and has an assembly cost of ∼$2500. This holographic imaging flow cytometer is based on color lens-free in-line holography, which is a computational imaging technique that uses partially coherent illumination light to capture holograms of flowing micro-objects on an image sensor, without the use of any lenses. These holograms are then digitally refocused and

https://dx.doi.org/10.1021/acsphotonics.1c00220
ACS Photonics XXXX, XXX, XXX−XXX

reconstructed computationally to generate color images of the objects within the sample, revealing both the amplitude and the phase information of the objects at three different color channels (red, green and blue). This field-portable imaging cytometer analyzes the objects within a water sample of interest in real time at a throughput of 100 mL/h with a half-pitch spatial resolution of <2 μm.

Here, we demonstrate new analysis methods that utilize this imaging flow-cytometer to perform an automated and high-throughput phenotypic inspection of microalgae populations in the presence of pollutants within the water sample. Figure 1 shows an overview of our methods. To enable the automated phenotypic analysis of microalgae populations, two different methods have been developed to analyze the algae passing through the flow cytometer. The first method directly performs a feature analysis (based on a few hand-crafted features) of the objects that the flow cytometer detects. By observing the statistical changes in these automatically extracted features, we can sense changes to the makeup of the algae passing through the cytometer. The second method classifies the species passing through the system using a set of three deep neural networks. This allows the system to accurately count the number of each algae species in a sample containing a mixture of algae species. Using these methods, the flow cytometer can be used to analyze microalgae populations under different environmental conditions.

We experimentally validated the performance of these methods by imaging four different species of algae passing through our label-free imaging cytometer under various culture conditions. The holographic images of these algae populations were analyzed by extracting features such as color intensity ratio, area, and circularity that were quantified to understand the effects of external perturbations due to different concentrations of copper. Interactions among different algae species were also analyzed using a medium perturbed by different copper concentrations, and the number of each algae species within the sample was estimated using a set of deep neural networks. While we performed these analyses using various toxic concentrations of copper to perturb the samples, the presented technique is broadly applicable to measuring the effects of other toxins/chemicals and other forms of perturbations (including e.g., mechanical) upon microalgae populations.

METHODS

Holographic Imaging Flow Cytometer Hardware. The holographic imaging flow cytometer facilitates a variable sample flow rate (1−100 mL/h) using a built-in peristaltic pump (Instech p625).[17,18] The continuously flowing liquid sample is illuminated by red (630 nm), green (530 nm), and blue (450 nm) light-emitting diodes (LED) that are pulsed (120 μs), and the holographic signatures of the flowing microalgae are recorded on a 14-megapixel image sensor (Basler aca4600-10uc) running in global reset release mode and triggering the LEDs. The housing of the camera was modified to allow the sample carrying flow channel (Ibidi, #80191, uncoated, channel height: 0.8 mm) to come into direct contact with the image sensor. The temporal and spatial coherence of the illumination is adjusted by a pair of triple bandpass filters (Edmund Optics #87-246, Chroma Inc. 69015m) and a convex mirror (Edmund Optics #64-061), respectively. The short illumination pulse necessitates a high-power LED (Ledengin LZ4-04MDPB), with driving currents ranging from 2 to 5 A, depending on the color. These components were attached to a custom-designed PCB. The brightness of the LEDs can be set by the user to reach adequate white balance, and the intensity is kept constant using a constant current LED driver (LT3797, Linear Technologies). The charge for these rapid, high current pulses is provided by three electrolyte capacitors with a total capacitance of 0.3 F charged to 12 V using a capacitor charge controller IC (LT3750, Linear Technologies). The light pulses are synchronized by the flash signal provided by the image sensor. The full field of view holograms are captured at a rate of three frames per second, and the default liquid flow speed used for all experiments was 100 mL/h. The controlling circuit is powered by a 5 V power source, and the power consumption of the device is ∼2.2 W. The image sensor is powered by the USB connection to the controlling computer and consumes an additional 2.8 W during the imaging operation.

Hologram Reconstruction. Due to the lens-free and in-line nature of the holographic imaging setup, the field of view of our device is the same as the area of the image sensor (∼30 mm^2).[16,17] Each frame contains the holographic signatures of the algae flowing above the image sensor. The holographic signatures of static objects in the channels are digitally removed by subtracting the background hologram, which is calculated as the average of the 20 preceding lens-free frames. The holograms of the individual objects are detected using the circular Hough transform.[17] The individual colors are extracted from the raw Bayer pattern image using a noninterpolation based demosaicking technique.[19] The focus height for each detected object is determined by a complex edge sparsity-based focus metric.[20] The three-dimensional location of each object in the field of view is tracked over consecutive frames and objects detected and reconstructed previously are removed from the list of objects of interest to avoid reconstructing and counting the same algae twice. The holograms of the remaining objects are up-sampled by a factor of 4 and reconstructed using the angular spectrum method.[21,22] During this reconstruction, the slight difference in the incidence angles of the illumination wavelengths and the dispersion of the materials in the optical path are taken into account by the transfer function. This process yields an in-focus color phase and amplitude image from each object entering the field of view.

In-line digital holographic reconstructions contain noise in their reconstructions, termed twin-image artifact, arising from the unknown phase distribution of the field at the hologram plane. In order to remove the twin image noise and provide accurate phase and intensity reconstructions of each object, our system uses a convolutional neural network (CNN) to perform the image reconstructions.[17] Once generated, these denoised color phase and intensity images are used to classify the algae populations, and after extraction of various selected features, to track the spatial and spectral changes of various algae populations.

Safety. All experimental work involving the algae cultures was performed in a Biosafety Level 2 (BSL2) laboratory and within a biosafety cabinet following the environmental, health, and safety rules of UCLA.

Culturing of Algae Species. We purchased the axenic algae species *D. tertiolecta* (CCMP1320), *Nitzschia* (CCMP1698), Bacillariophyceae (CCMP2024), and *Thalassiosira* (CCMP2929) from Bigelow National Center for Marine Algae and Microbiota (NCMA; Maine, U.S.A.) and used L1

https://dx.doi.org/10.1021/acsphotonics.1c00220
ACS Photonics XXXX, XXX, XXX−XXX

medium as the growth media (Table S1).[23] Axenic starter cultures of the species were used to ensure sample purity. L1 medium was prepared using a kit (product no. MKL150L, Bigelow NCMA, Maine, U.S.A.) according to the instructions of the manufacturer. This process involves adding 1 mL from each stock solution, except the vitamin stock (i.e., added 0.5 mL) into filtered seawater (product no. SEABH20L, Bigelow NCMA, Maine, U.S.A.), after which the pH of the medium was adjusted to 8.0, and the medium was sterilized. The species were incubated at 25 ± 0.4 °C on a custom-designed shaker incubator at 100 rpm under continuous illumination of white LED array lighting at ∼90 $\mu E/m^2/s$.

Design of the Incubator for Algae Growth. The incubator used to grow the algae is a shaker incubator (product no. 31412, Genesee Scientific, California, U.S.A.) with the door removed, and replaced with a custom-designed acrylic door. The acrylic panels were cut and patterned using a laser cutter (Speedy 100, Trotec Laser Inc., Michigan, U.S.A.) and glued to each other to form a custom-designed door. The door had an opening on top which held an LED array (product no. B079J5YCHT, Amazon Inc., U.S.A.) for uniform illumination, two fans (product no. B0119SLG18, Amazon Inc.) on the sides, and holes for air circulation.

Sample Preparation. We used cultured species that are 4−7 days old to prepare algae samples. The test solution volume was 15 mL and contained within a 25 mL vial. The test solutions were not renewed unless otherwise stated (in other words, the tests were static nonrenewal). We used copper(II) chloride dihydrate ($CuCl_2 \cdot H_2O$; product no. C3279−100G, Sigma-Aldrich) to analyze the effect of copper on the growth of algae species. A total of 0.170 g of $CuCl_2 \cdot H_2O$ was added in reagent grade water and then the suspension was diluted using L1 medium to have different concentrations of copper (Cu^{2+}) containing medium. The copper concentrations used were 0.63 (0.0006 ppm), 63.6 (0.0636 ppm), 630 (0.63 ppm), and 6300 $\mu g/L$ (6.3 ppm), depending on the experiment being performed. Copper is one of the essential components of the L1 medium, therefore, 0.63 $\mu g/L$ concentration was used as the control concentration of Cu^{2+} throughout this study. The initial concentration of algae in the test samples was adjusted to 10^4 cells/mL using a count obtained from a hemocytometer. The added algae stock volume to each test flask was not more than 1 mL at all measurements. We added 14 mL of medium and 1 mL of algae stock into each flask and mixed the suspension gently.

We diluted 500 μL from each test flask into 9.5 mL of L1 medium for each test sample. The experiments with a single copper exposure were conducted in duplicate for algae monoculture experiments (except Day 1−63 $\mu g/L$ of *D. tertiolecta* that was performed a single time due to experimental error), and all mixture experiments with a single copper exposure were performed in triplicate. The experiments with multiple copper exposures were all conducted in triplicate. Each of the flasks was rotated daily to ensure uniform illumination and temperature in the custom-made shaker incubator.

Image Segmentation and Feature Extraction. Analysis of the spatial and spectral features of algae passing through the cytometer was used to investigate the effects of different perturbations to the algae cultures as well as to probe the interactions between different algae species. To perform this analysis, an automated workflow was implemented in MATLAB R2018a (see Figure S2). This workflow begins with the application of an adaptive segmentation algorithm to the reconstructed intensity and phase images containing individual objects. The features used for analysis of the algae are then extracted using the resulting segmentation map. To perform this adaptive segmentation, Canny edge detection was first applied to the intensity and phase images.[24] Canny edge detection smoothens the image with a Gaussian filter that has a specified standard deviation (in our case, it is selected as 2.4 pixels). Using the smoothed image, the intensity gradients are computed. After applying nonmaximal suppression to make the edges thinner, a double threshold ([0.1, 0.12]) is used to obtain more accurate edges. Finally, edge linking is performed to find the weak edge pixels that are connected to the strong edge pixels. The edge maps of the reconstructed intensity and phase images alongside their combination with a bitwise "OR" operation are used to obtain three distinct segmentation maps by applying a 10 pixel dilation, filling holes using the flood-fill algorithm,[25] and 10 pixel erosion, respectively. These segmentation maps are combined with a bitwise "OR" operation to obtain the final segmentation result.

Using the resulting segmentation maps, several spatial features (e.g., area, perimeter, circularity, eccentricity, axis ratio (major/minor axis)) and spectral features (e.g., brightness, color intensity ratios (blue/green and red/green)) of algae or nonalgae objects are extracted. For each image, average red, green, and blue intensities for segmented regions are obtained from intensity images and normalized with respect to the average background brightness. These values are used to obtain the color intensity ratios and brightness. Several spatial features including eccentricity, major and minor axis lengths are obtained by using an ellipse that has the same normalized second central moments as the segmented region.[26] Eccentricity is determined as the ratio of the distance between the foci of the ellipse and its major axis length. Therefore, this eccentricity ratio is between 0 (ideal circle) and 1 (line segment). Major and minor axis lengths of the ellipse are used to obtain the axis ratio. Area and perimeter of the detected algae are also directly quantified by using the segmented images. Moreover, circularity of each object is obtained by using the following equation:

$$\text{circularity} = 4\pi \cdot \text{area} \Big/ \text{perimeter}^2 \tag{1}$$

which is defined to give a value of 1 for completely circular objects and smaller values for noncircular objects. However, since the perimeter is not approximated well in digital images, the equation might give values slightly higher than 1.[27]

Normalization of Histograms. The reported histograms were normalized to obtain probability density functions (PDFs) using the following equation:

$$v_i = \frac{c_i}{N \cdot w_i} \tag{2}$$

where v_i denotes the value of i^{th} bin in a histogram, c_i represents the number of elements in the bin, w_i represents the width of the bin, and N represents the number of total elements in the histogram.

Quantification of Similarity between Measured PDFs. Kullback−Leibler (KL) divergence (D_{KL}) was used to quantify the similarity between the measured PDFs,[28] defined as

$$D_{KL}(p(x)||q(x)) = \sum_{x \in X} p(x) \ln \frac{p(x)}{q(x)} \tag{3}$$

https://dx.doi.org/10.1021/acsphotonics.1c00220
ACS Photonics XXXX, XXX, XXX−XXX

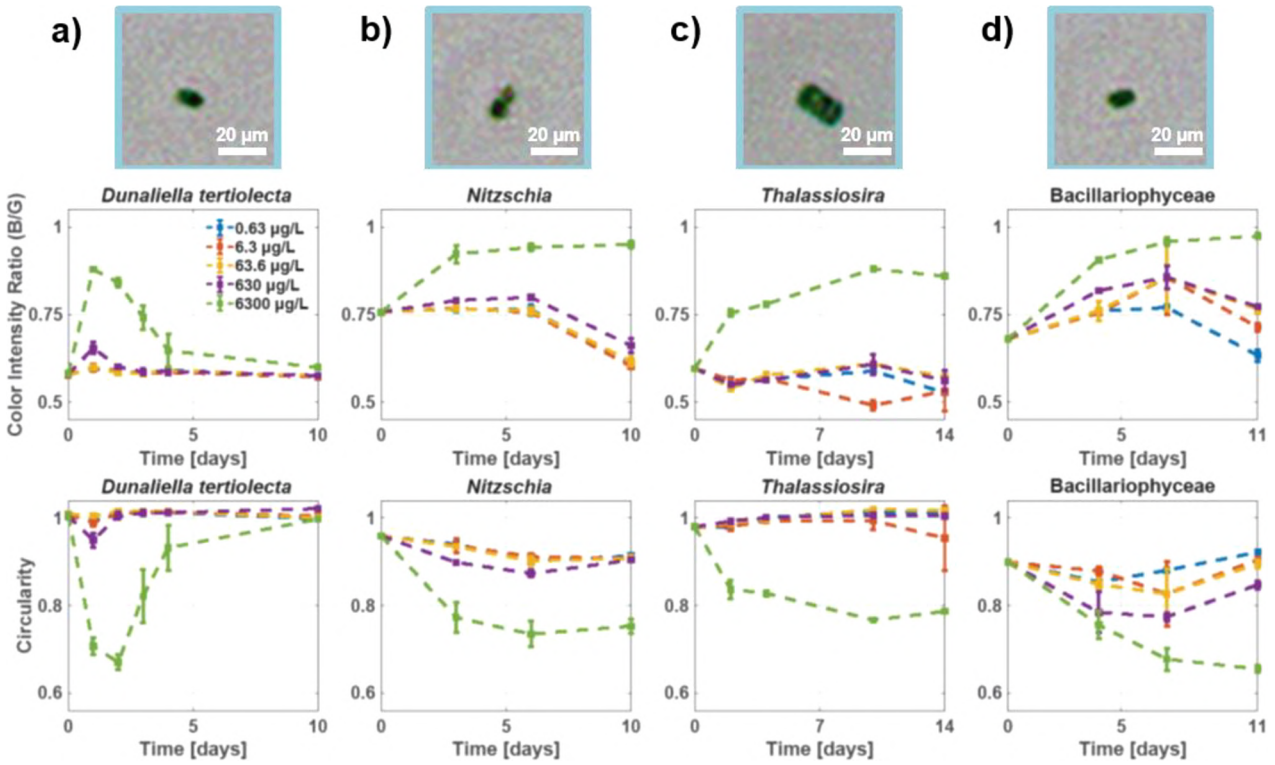

Figure 2. Effects of copper exposure on four different algae monocultures monitored over time using the holographic imaging flow cytometer. Various concentrations of copper are introduced into the algae monocultures at day 0, and the samples are measured at regular time intervals by the imaging flow cytometer. The device analyses ~5000−15000 individual algae images per measurement. Two of the monitored features, color intensity ratio (blue/green) and circularity, are displayed here to visualize the effect of various copper concentrations over time. The median values of the measured features for each day and copper concentration are shown. The error bars indicate the standard deviation from repeated runs of the experiments. As the spiked copper concentration increases from the typical 0.63 μg/L in the growth medium (blue), an increased divergence from the control sample can be seen.

where $p(x)$ and $q(x)$ are probability distributions. As KL divergence is a nonsymmetric distance metric, its symmetric counterpart (Jeffreys divergence) was used for the analysis.[29] Jeffreys divergence is defined as

$$\mathrm{SymKL} = 0.5 \times (D_{\mathrm{KL}}(p(x)||q(x)) + D_{\mathrm{KL}}(q(x)||p(x))) \tag{4}$$

As symmetric KL divergence ranges between 0 and infinity, it was normalized between 0 and 1 using the equation below to make the KL divergence easier to visually compare:

$$\mathrm{KL} = 1 - e^{-\mathrm{SymKL}} \tag{5}$$

Classification of Algae Using Convolutional Neural Networks. A set of three deep neural networks were used in conjunction to perform the classification of the microalgae population in each sample and differentiate between different algae species. Each of these neural networks was used to classify a specific type of algae. In other words, each trained neural network differentiates between two classes: (1) the algae species corresponding to that network and (2) every other object (i.e., other algae types, nonalgae particles, and severely damaged algae from other species). When training each network, only healthy algae of the type corresponding to the network were classified as part of the first class (i.e., the network should identify only the algae species corresponding to that network). A mixture of "other" objects, consisting of the other algae types (both healthy and damaged by a high concentration of copper), alongside other nonalgae objects (e.g., dirt, dust), was used as the second class. This training regime is necessary as generating labels, for example, marking damaged and dead algae is an intractable problem due to the variations in the amount of damage that can be done to algae within a sample, in addition to the natural variations observed. These ground truth labels were used by a softmax cross-entropy loss function to train each one of these algae specific neural networks. Using these labels, the loss for the network corresponding to algae N can be described as follows:

$$L_{\mathrm{algae}N} = -y_{c=\mathrm{algae}N} \log(p_{c=\mathrm{algae}N}) - y_{c=\mathrm{other}} \log(p_{c=\mathrm{other}}) \tag{6}$$

where y_c is a one-hot encoded binary encoding of the label, which has a value of one when the object belongs to that class, and zero otherwise. The p_c probabilities were calculated by passing the network output through the softmax function below, where k is the class index:

$$p_c = \frac{\exp(z_c)}{\sum_{k=1}^{2} \exp(z_{c=k})} \tag{7}$$

p_c represents the probabilities estimated by the neural network that the object being classified belongs to the class corresponding to c.

When classifying individual species in a mixture, all of these networks are applied at the same time. If one of the networks classifies the object as the algal cell, it is marked as the algae type corresponding to that network. If none of the networks classify it is as algal cell, the object is marked as nonalgal cell. In the case where multiple networks classify an object as the

https://dx.doi.org/10.1021/acsphotonics.1c00220
ACS Photonics XXXX, XXX, XXX−XXX

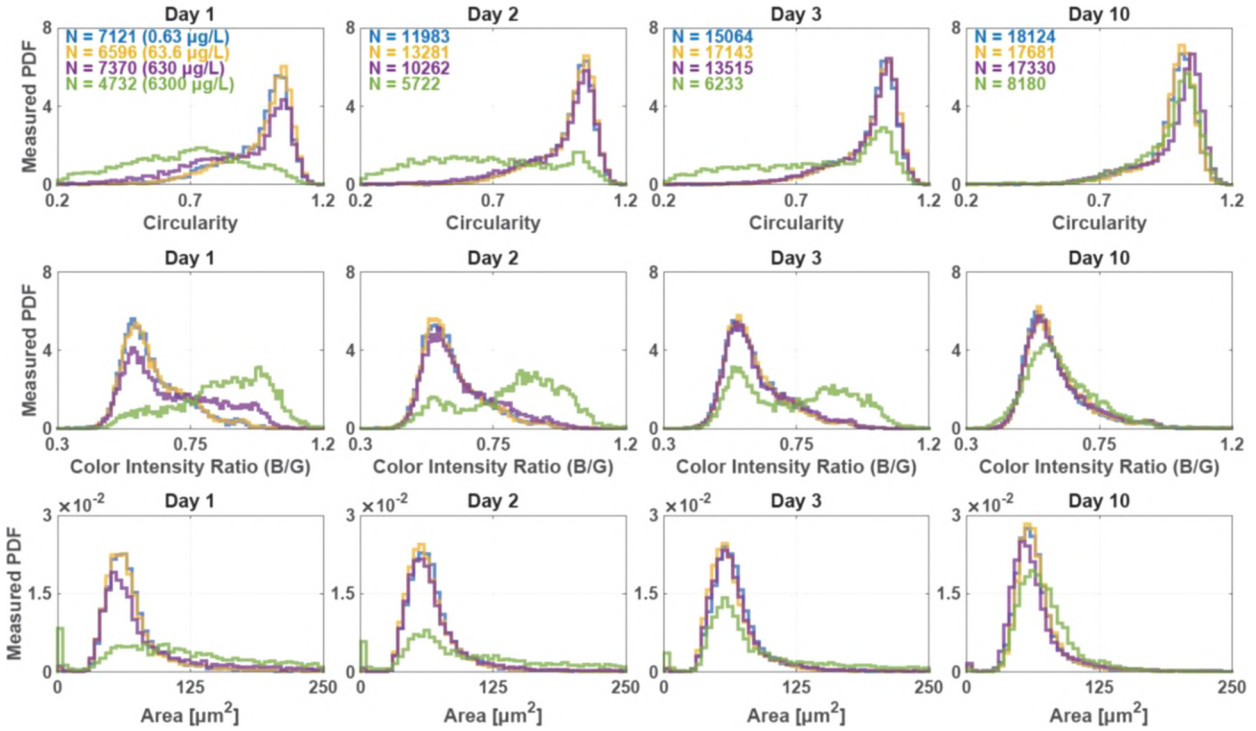

Figure 3. Normalized histograms (measured PDFs) of the circularity, color intensity ratio, and area of the imaged algae (*Dunaliella tertiolecta*) as a function of copper concentration. The PDFs of three features (i.e., circularity, blue/green color intensity ratio and area of algae) are displayed to help visualizing the effect of the copper concentration over time. For this species, a significant divergence from the histogram of the control sample can be observed for higher copper concentrations.

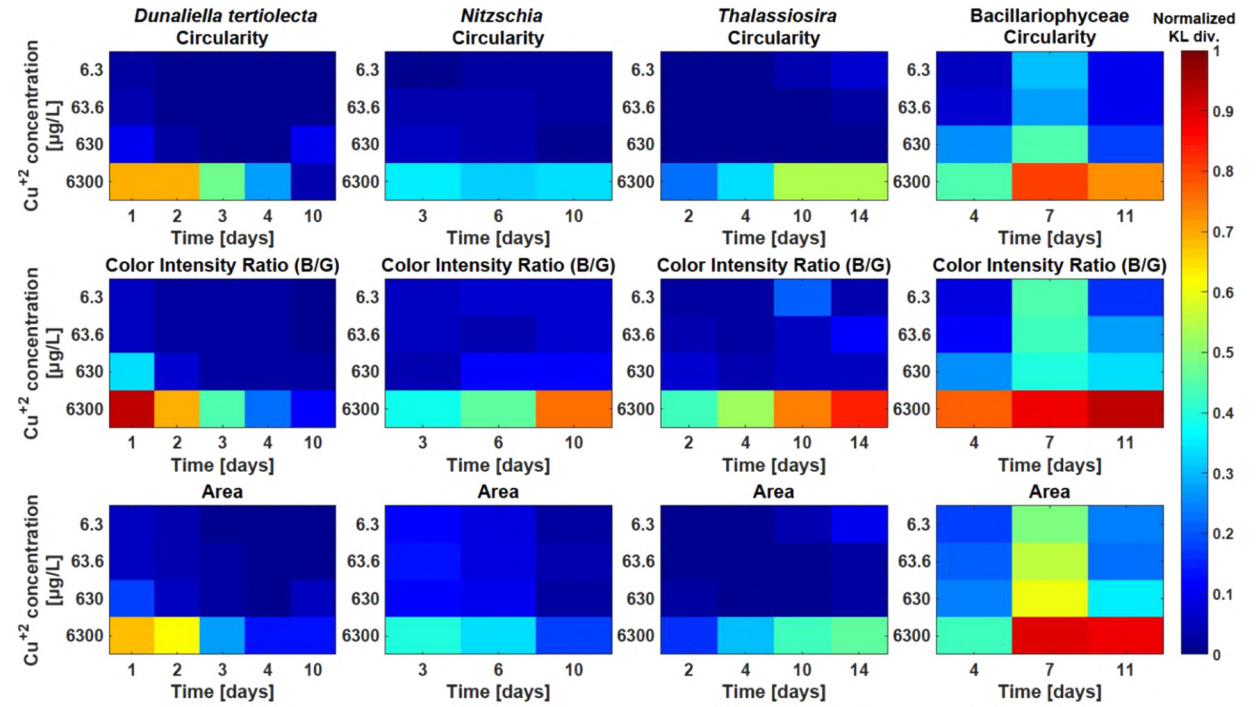

Figure 4. KL divergence analysis on the impact of copper concentration over time. The normalized symmetric KL divergence values are shown to quantitatively measure the difference between the measured PDFs of the selected features for the control (0.63 μg/L copper concentration) and the higher copper concentrations. Blue color represents a small difference, while red color corresponds to a large difference. This figure also highlights the difference in copper sensitivity among species.

alga, the cell is classified according to whichever network had the highest confidence in its inference. A block diagram outlining the operation of the three networks is reported in Supporting Information, Figure S2.

https://dx.doi.org/10.1021/acsphotonics.1c00220
ACS Photonics XXXX, XXX, XXX−XXX

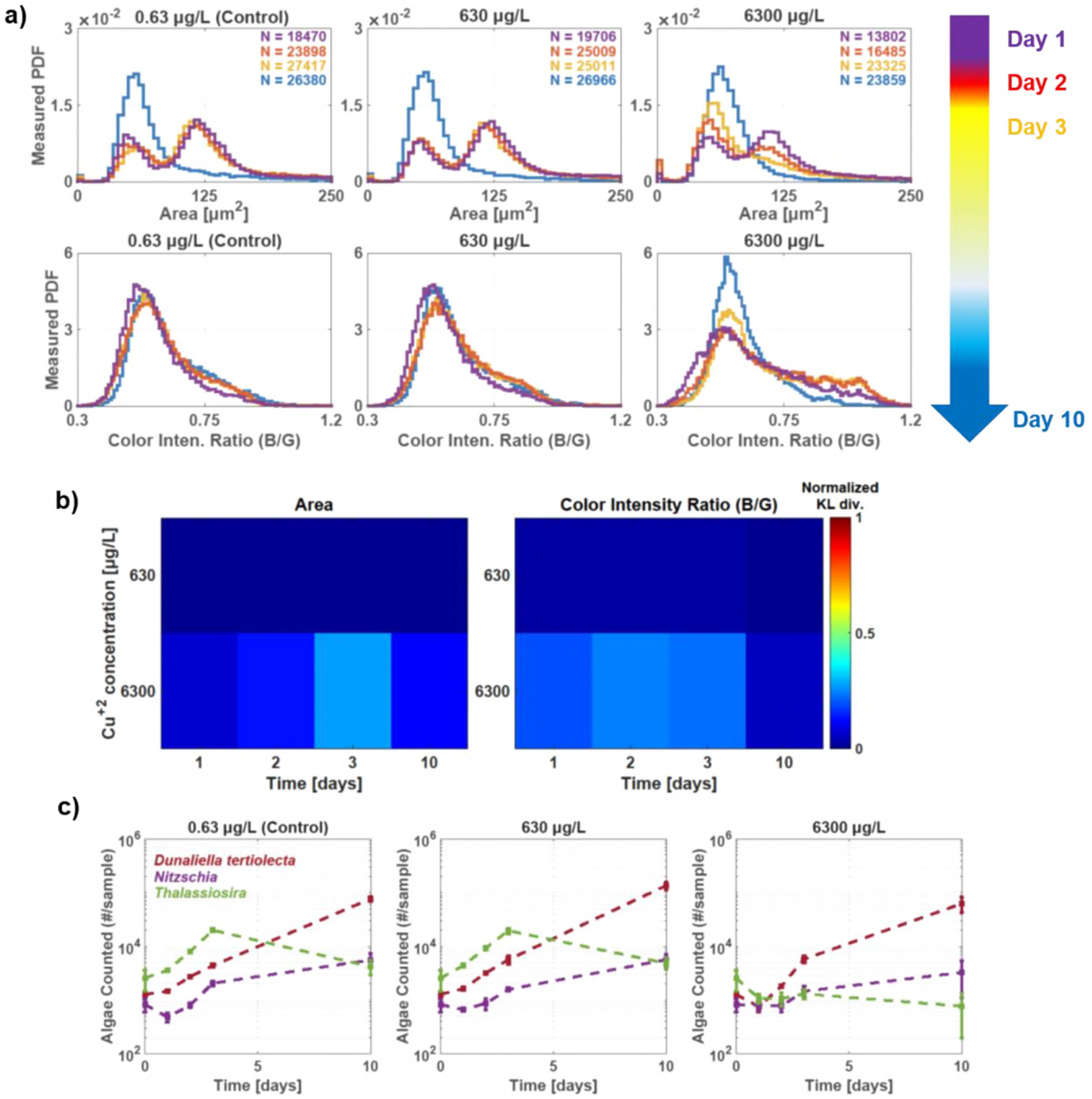

Figure 5. Algae mixture experiments (*D. tertiolecta*, *Nitzschia*, and *Thalassiosira*). (a) A comparison of the PDFs for color intensity ratio (blue/green) and area as a function of the copper concentration over time. (b) Normalized KL divergence between different copper concentrations and the control (0.63 μg/L copper concentration). (c) Number of detected algae for each algae species within the mixtures. *D. tertiolecta* eventually dominated the mixture due to its superior copper tolerance and growth rate.

All of the networks use the same architecture (densenet-121[30]) and are used to classify 256 × 256 pixel-sized images containing the algae. Each of these image patches contains six unique information channels, three amplitude and three phase channels, corresponding to the red, green, and blue channels. The *D. tertiolecta* network was trained for 140 epochs using 14057 images of this algae type and 25180 images of other algae and nonalgae. The *Nitzschia* network was trained for 129 epochs using 9258 images of this algae type and 32952 images of other algae and nonalgae. Finally, the *Thalassiosira* network was trained for 160 epochs using 7787 images of this algae type and 34423 images of other algae and nonalgae. A total of 80% of the images in each case were used for training, while the remaining 20% were used for validation. The classification networks were trained and implemented using Python version 3.6.2 and using Pytorch version 1.2 using a Nvidia GTX 1080Ti GPU.

When the three networks are used in conjunction, they misclassified 5.5%, 3.3%, and 2.4% of the *D. tertiolecta*, *Nitzschia*, and *Thalassiosira* algae, respectively. These tests were performed on 1000 blindly tested objects from the same monoculture samples.

RESULTS

Effect of Copper Exposure to Microalgae Monocultures. The flow cytometer system utilizing the feature extraction algorithm was tested on algae monocultures from four different species (*D. tertiolecta*, *Nitzschia*, *Thalassiosira*, and *Bacillariophyceae*), which were selected according to their purity, shape, and size. Their individual responses to copper exposure at various concentration levels over time were analyzed by comparing different features such as circularity, eccentricity, area, and blue/green color intensity ratio extracted

https://dx.doi.org/10.1021/acsphotonics.1c00220
ACS Photonics XXXX, XXX, XXX−XXX

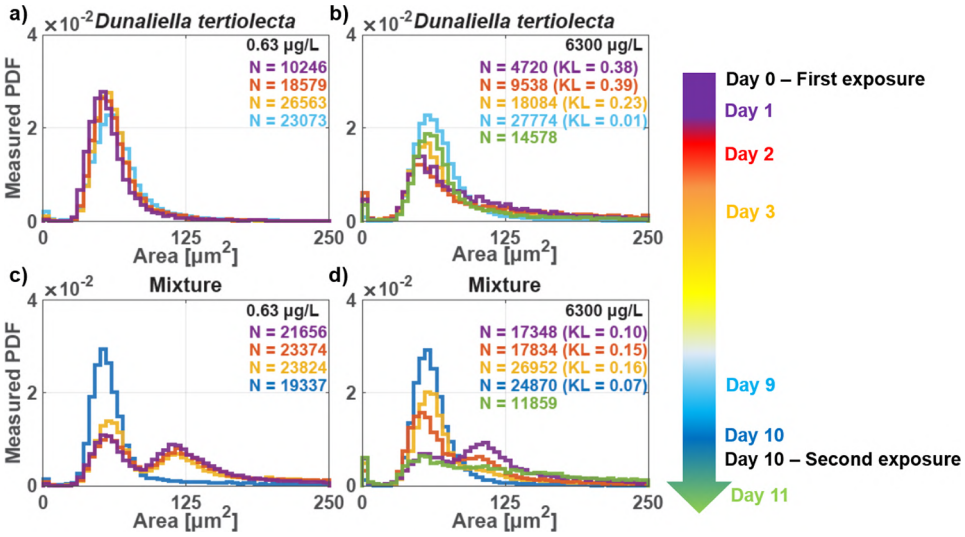

Figure 6. Impact of multiple copper exposure over time for *Dunaliella tertiolecta* and algae mixture. A comparison of the PDFs of algae area as a function of the copper concentration over time. (a and b) Area of the objects measured in the *Dunaliella tertiolecta* monoculture at the control concentration (0.63 μg/L) and the highest copper concentration (6300 μg/L), respectively. (c and d) Area of the objects measured in the mixture sample (*Dunaliella tertiolecta*, *Nitzschia*, and *Thalassiosira*) at the control concentration (0.63 μg/L) and the highest copper concentration (6300 μg/L), respectively. For the algae mixture, the change in area measured by the system due to the second exposure is larger than that of the *Dunaliella tertiolecta* monoculture, even though *Dunaliella tertiolecta* makes up nearly the entire sample on day 10.

by the feature extraction algorithm. The time evolution of the median values of two features (i.e., circularity and blue/green color intensity ratio) at various initially spiked copper concentrations are illustrated in Figure 2. These two features were found to be the most sensitive indicators of copper exposure, while other features were affected by the spiked copper to varying lesser degrees (the effects of copper on other features are reported in Figures S3 and S4). Small standard deviations between the median values of these features across repeated experiments demonstrate the repeatability of the overall method, which stems from the high throughput nature of our lens-free imaging flow cytometer, enabling it to image and analyze thousands of algae from each sample.

To better visualize and quantify the effect of copper exposure on the algae, we also performed both a direct comparison of the normalized histograms of these features (see Figures 3 and S5–S7) as well as a KL divergence analysis of these histograms (see Figure 4). This analysis can be used to measure the dissimilarity between the control samples containing 0.63 μg/L copper and the samples spiked with higher concentrations of copper. Analyzing KL divergence values can give more accurate and sensitive comparisons than simply analyzing changes to the median feature values as it is computed using the entire set of data rather than relying upon a single-point estimation.

Our measurements and related analyses reveal that *D. tertiolecta*[7] is the most copper-tolerant of the four algae species tested (see Figures 2a, 3a, and 4). For this type of algae, we only detect changes at the higher copper concentrations (i.e., a small change can be seen for 630 μg/L exposure and a larger change can be seen for 6300 μg/L exposure). Furthermore, on the 10th day, the observed features returned to the same state as the control samples. This is likely due to the copper concentration diminishing over time as the metal adsorbs to the cell surface of the dead algae, and the surviving algae multiplying to repopulate the sample. The species *D. tertiolecta*, *Nitzschia*, and *Thalassiosira* also appear to be less susceptible to lower copper concentrations as indicated by the relatively small deviations observed in the tracked features (see Figures 2a–c and 4). At the highest copper concentration level, the observed features of *Nitzschia* and *Thalassiosira* did not return to the same state as the control samples within the 10-day experiment, indicating that these algae species continue to be affected by the copper after a longer period than *D. tertiolecta*. The remaining algae species, Bacillariophyceae, showed a slower response time to the same copper concentrations and appeared to be more susceptible to the lower copper concentrations, as shown by Figures 2d and 4.

Observation of Microalgae Features and Population Dynamics in Mixed Cultures. The individual response of an algae species to different copper concentration levels in a mixed culture is different than that of a monoculture due to the interactions among different species in the mixture. Therefore, the flow cytometer utilizing the feature extraction and deep learning-based classification algorithms was used to analyze the effects of different copper concentrations on algae species within a mixed culture. For this, mixed cultures of microalgae populations composed of three species of algae, *D. tertiolecta*, *Nitzschia*, and *Thalassiosira*, at three different copper concentrations (0.63 (control), 630, and 6300 μg/L) were used. For this mixture experiment, the sample composition was analyzed both by the feature extraction algorithm used to analyze the algae monocultures and by using our deep learning-based algae classification algorithm (see Methods). This algae classification was used to detect relative changes in the populations as well as the growth of different species over time. This deep learning-based technique classifies individual algae species in the mixture using three CNNs in conjunction, where each of the network models works as a binary classifier for each of three species in the mixture. Using this method, the networks can be trained to classify healthy algae correctly, while marking severely damaged or dead algae as nonalgae. Using our approach, damaged algae are considered to be nonalgae when all the three classification networks rate them as

https://dx.doi.org/10.1021/acsphotonics.1c00220
ACS Photonics XXXX, XXX, XXX–XXX

more closely matching the sample distribution of "non-algae" class. Therefore, the need for the correct labeling of the damaged algae is eliminated altogether.

Using both the feature extraction and classification techniques, we were able to show that *D. tertiolecta* eventually dominates the other species regardless of the copper concentration being studied. This is revealed both by the classification of the objects passing through the cytometer (Figure 5c) as well as the histograms of algae size (Figure 5a). As *Thalassiosira* is a larger species than *D. tertiolecta* and *Nitzschia*, which have similar sizes (see Table S1), the disappearing (right) peak in Figure 5a corresponds to a relative reduction in the concentration of *Thalassiosira*. In this experiment, the copper tolerance and higher growth rate of *D. tertiolecta* allowed it to eventually make up the majority of the algae within the system. Note that, at the highest copper concentration (6300 μg/L), the domination of *D. tertiolecta* within the mixture occurred faster. The KL divergence analysis for the mixture experiments shown in Figure 5b further supports these observations.

Impact of a Second Exposure to Copper on Microalgae Cultures. The effects of a second copper exposure to both an algae monoculture and an algae mixture were analyzed using the same methods described above. As in the case of the previous mixture experiment, this algae mixture contained three species (*D. tertiolecta*, *Nitzschia*, and *Thalassiosira*), while *D. tertiolecta* was used for the monoculture experiments. In all these experiments, in addition to the initial 6300 μg/L spiking of copper (using the same process as previously described experiments), the test samples were further spiked with copper for a second time on Day 10.

Similar to the mixture experiments discussed in the previous section, *D. tertiolecta* dominated the other two algae 10 days after exposure. When the copper concentration of the mixed culture was brought to 6300 μg/L for a second time, we observed large changes in the extracted features, which indicates that the algae did not develop any significant tolerance to copper (Figure S9a,b). When the same experiment was performed for a monoculture containing only *D. tertiolecta*, as seen in Figure S8, the second copper exposure has a smaller effect upon the median feature values for this monoculture. Furthermore, the changes are much smaller for the monoculture than for the algae mixture. To visualize the effects of the second exposure on *D. tertiolecta* and algae mixture, histograms of the area of algae over time are shown in Figure 6, which reveal that the second copper exposure affects the algae mixture more than the algae monoculture. This indicates that the *D. tertiolecta* algae grown in the mixture develop less of a resistance to copper than those grown in a monoculture, possibly due to the other two more affected algae types absorbing some of the initially spiked copper. Histograms showing the same effects for additional features are further reported in Figures S10 and S11.

DISCUSSION

This presented imaging flow-cytometer is capable of performing high-throughput analysis of microscopic objects, which allows a 10 mL sample to be measured in ~6 min. Consequently, when used in conjunction with feature extraction and deep learning-based algae classification methods, as demonstrated in this work, our cost-effective and field-portable flow cytometer outperforms commonly used cell counting methods such as hemocytometers in terms of time savings, accuracy, and ease of use. In addition, manual counting using a hemocytometer has limitations on the sample concentration that can be measured. For instance, while the lowest concentration that can be measured by traditional hemocytometers is around 10^4 cells/mL, a concentration of 2.5×10^5 cells/mL is usually considered as the lower limit for accurate counting of cells using this method.[31] Our flow cytometer provides a high-throughput method to detect and count cells in a suspension, also covering much lower concentrations.[32] Another major advantage of using our flow-cytometer over manual counting is that it can image, detect, and count motile cells such as *D. tertiolecta*, as the illumination pulse during frame capture is only ~0.1 ms. Manual counting of motile specimens under a benchtop microscope is difficult to perform and can be inaccurate as they move in and out of focus and the imaging field of view.

In contrast to traditional imaging flow cytometers, which use a fluorescent trigger to image cells of interests, our device does not rely on fluorescence or other labels to facilitate image capture, consequently, it images every object in the liquid sample. There is no need for fluorescence tagging, or any chemical pretreatment, and the technique works, regardless of whether the sample of interest has autofluorescence or not. This allows it to measure both live and remnants of dead algae, and due to its ability to capture both the intensity and phase images, it can detect and image otherwise transparent objects such as the shells of diatoms. Furthermore, since our device does not require any sample preparation and can image/analyze the water sample under test without modifying it, it is nondestructive and nonpolluting. Consequently, it can release the sample back to the environment after analysis, which makes our technology able to ultimately be deployed in the field to monitor a body of natural water remotely and automatically. The cost-effective nature and the low hardware complexity of the technology make it especially promising to serve as an element of an interconnected, distributed sensor network to monitor a larger area.

Through our experiments and analyses, we demonstrated that our method can measure and track the response of algae populations to perturbations such as the addition of toxic levels of copper. Changes in the algae composition, count, and the measured spatial/spectral features can be used to indicate the presence of any arbitrary contaminant affecting the population. This contrasts with more traditional sensors that are specific for an individual analyte. This nonspecific nature of our detection system makes our technique applicable to detect unknown perturbations to the healthy state of the environment, making it ideal for an early warning system to direct more specific monitoring efforts to an area in cases where a major deviation from the natural state is detected. We believe that with enough experimental data it may be possible to distinguish the effects of various contaminants on the algae population from each other, thus, increasing the specificity of our technique.

Our device relies on computational imaging to obtain the phase and amplitude images of the flowing samples without the need for any lenses. Real-time operation is achieved by using the massively parallel computing capability of the controlling laptop's Nvidia graphics processing unit (GPU). The image quality and imaged volume per frame are determined by the pixel size and field-of-view of the image sensor, whereas the throughput is connected to the processing power of the GPU. Both of these key hardware components are evolving at a rapid

https://dx.doi.org/10.1021/acsphotonics.1c00220
ACS Photonics XXXX, XXX, XXX−XXX

pace, fueled by the growth and demand of the consumer electronics industry. Therefore, the capabilities of our imaging cytometer technology have the potential to further improve at a similar pace.

In summary, in this proof of principle study, we used a low-cost, field-portable, and high-throughput imaging flow cytometer to perform phenotypic analysis of microalgae populations using feature extraction and deep learning-based classification methods. Fully automated analysis was performed by extracting the spatial and spectral features of the reconstructed holographic images of the algae to observe and track the effects of any perturbations on these features as well as counting and classification of the algae within the sample using a set of CNNs. The effectiveness of this technique was experimentally proven by detecting perturbations caused by different copper concentrations within microalgae monocultures and mixtures of three algae species. By achieving automated phenotypical analysis of microalgae suspensions at a flow rate of 0.1 L/h without any labels or any damage/contamination to the sample, we believe that this imaging flow cytometry powered with deep learning provides a unique analytical tool for high-throughput inspection of water samples, even in field settings.

■ ASSOCIATED CONTENT

Supporting Information

The Supporting Information is available free of charge at https://pubs.acs.org/doi/10.1021/acsphotonics.1c00220.

Holographic imaging flow cytometer (Figure S1); Image processing pipeline and neural network-based classification (Figure S2); Effects of copper exposure on different features of four different algae monocultures monitored over time using the holographic imaging flow cytometer (Figures S3 and S4); Normalized histograms (measured PDFs) of color intensity ratio, circularity, and area of algae at different copper concentrations for different algae species (Figures S5−S7); Effects of multiple copper exposure on *Dunaliella tertiolecta* (Figure S8); Effects of multiple copper exposure on an algae mixture containing *Dunaliella tertiolecta*, *Nitzschia*, and *Thalassiosira* (Figure S9); Effects of multiple copper exposure on the PDFs of different features for *Dunaliella tertiolecta* and an algae mixture (*Dunaliella tertiolecta*, *Nitzschia*, *Thalassiosira*; Figures S10 and S11); Images of studied algae species captured using a regular brightfield microscope (Figure S12); The algae species used in our experiments and their properties (Table S1) (PDF)

■ AUTHOR INFORMATION

Corresponding Author

Aydogan Ozcan − *Electrical and Computer Engineering Department, Bioengineering Department, and California NanoSystems Institute (CNSI), University of California, Los Angeles, California 90095, United States;* orcid.org/0000-0002-0717-683X; Phone: +1(310)825-0915; Email: ozcan@ucla.edu; Fax: +1(310)206-4883

Authors

Çağatay Işıl − *Electrical and Computer Engineering Department, Bioengineering Department, and California NanoSystems Institute (CNSI), University of California, Los Angeles, California 90095, United States;* orcid.org/0000-0003-3367-1858

Kevin de Haan − *Electrical and Computer Engineering Department, Bioengineering Department, and California NanoSystems Institute (CNSI), University of California, Los Angeles, California 90095, United States*

Zoltán Göröcs − *Electrical and Computer Engineering Department, Bioengineering Department, and California NanoSystems Institute (CNSI), University of California, Los Angeles, California 90095, United States*

Hatice Ceylan Koydemir − *Electrical and Computer Engineering Department, Bioengineering Department, and California NanoSystems Institute (CNSI), University of California, Los Angeles, California 90095, United States*

Spencer Peterman − *Bioengineering Department, University of California, Los Angeles, California 90095, United States*

David Baum − *Electrical and Computer Engineering Department, University of California, Los Angeles, California 90095, United States*

Fang Song − *Electrical and Computer Engineering Department, University of California, Los Angeles, California 90095, United States*

Thamira Skandakumar − *Bioengineering Department, University of California, Los Angeles, California 90095, United States*

Esin Gumustekin − *Neuroscience Department, University of California, Los Angeles, California 90095, United States*

Complete contact information is available at: https://pubs.acs.org/10.1021/acsphotonics.1c00220

Author Contributions

†These authors contributed equally to this work.

Notes

The authors declare the following competing financial interest(s): A.O. is a co-founder of Lucendi Inc., a company that commercializes computational microscopy tools.

■ ACKNOWLEDGMENTS

The authors acknowledge funding from the Intelligence Advanced Research Projects Activity (IARPA).

■ REFERENCES

(1) Field, C. B.; Behrenfeld, M. J.; Randerson, J. T.; Falkowski, P. Primary Production of the Biosphere: Integrating Terrestrial and Oceanic Components. *Science* **1998**, *281* (5374), 237−240.

(2) Ali, H.; Khan, E. Trophic Transfer, Bioaccumulation, and Biomagnification of Non-Essential Hazardous Heavy Metals and Metalloids in Food Chains/Webs—Concepts and Implications for Wildlife and Human Health. *Hum. Ecol. Risk Assess.* **2019**, *25* (6), 1353−1376.

(3) Anu, P. R.; Bijoy Nandan, S.; Jayachandran, P. R.; Don Xavier, N. D. Toxicity Effects of Copper on the Marine Diatom, Chaetoceros Calcitrans. *Reg. Stud. Mar. Sci.* **2016**, *8*, 498−504.

(4) Overnell, J. The Effect of Heavy Metals on Photosynthesis and Loss of Cell Potassium in Two Species of Marine Algae, Dunaliella Tertiolecta and Phaeodactylum Tricornutum. *Mar. Biol.* **1974**, *29* (1), 99−103.

(5) Davis, A. K.; Hildebrand, M.; Palenik, B. Gene Expression Induced by Copper Stress in the Diatom Thalassiosira Pseudonana. *Eukaryotic Cell* **2006**, *5* (7), 1157−1168.

(6) Miller, K. A.; Thompson, K. F.; Johnston, P.; Santillo, D. An Overview of Seabed Mining Including the Current State of Development, Environmental Impacts, and Knowledge Gaps. *Front. Mar. Sci.* **2018**, *10*, 4.

(7) Levy, J. L.; Stauber, J. L.; Jolley, D. F. Sensitivity of Marine Microalgae to Copper: The Effect of Biotic Factors on Copper Adsorption and Toxicity. *Sci. Total Environ.* **2007**, *387* (1), 141−154.
(8) Gustavson, K.; Petersen, S.; Pedersen, B.; Stuer-Lauridsen, F.; Pedersen, S.; Wängberg, S.-Å. Pollution-Induced Community Tolerance (PICT) in Coastal Phytoplankton Communities Exposure to Copper. *Hydrobiologia* **1999**, *416* (0), 125−138.
(9) Levy, J. L.; Angel, B. M.; Stauber, J. L.; Poon, W. L.; Simpson, S. L.; Cheng, S. H.; Jolley, D. F. Uptake and Internalisation of Copper by Three Marine Microalgae: Comparison of Copper-Sensitive and Copper-Tolerant Species. *Aquat. Toxicol.* **2008**, *89* (2), 82−93.
(10) Filimonova, V.; Gonçalves, F.; Marques, J. C.; De Troch, M.; Gonçalves, A. M. M. Biochemical and Toxicological Effects of Organic (Herbicide Primextra® Gold TZ) and Inorganic (Copper) Compounds on Zooplankton and Phytoplankton Species. *Aquat. Toxicol.* **2016**, *177*, 33−43.
(11) Magnusson, M.; Heimann, K.; Ridd, M.; Negri, A. P. Chronic Herbicide Exposures Affect the Sensitivity and Community Structure of Tropical Benthic Microalgae. *Mar. Pollut. Bull.* **2012**, *65* (4), 363−372.
(12) Cid, Á.; Prado, R.; Rioboo, C.; Suárez-Bregua, P.; Herrero, C. *Use of Microalgae as Biological Indicators of Pollution: Looking for New Relevant Cytotoxicity Endpoints*; Nova Science Publishers, 2012; pp 311−323.
(13) Dashkova, V.; Malashenkov, D.; Poulton, N.; Vorobjev, I.; Barteneva, N. S. Imaging Flow Cytometry for Phytoplankton Analysis. *Methods* **2017**, *112*, 188−200.
(14) Taucher, J.; Haunost, M.; Boxhammer, T.; Bach, L. T.; Algueró-Muñiz, M.; Riebesell, U. Influence of Ocean Acidification on Plankton Community Structure during a Winter-to-Summer Succession: An Imaging Approach Indicates That Copepods Can Benefit from Elevated CO2 via Indirect Food Web Effects. *PLoS One* **2017**, *12* (2), No. e0169737.
(15) Poulton, N. J. FlowCam: Quantification and Classification of Phytoplankton by Imaging Flow Cytometry. *Methods Mol. Biol.* **2016**, *1389*, 237−247.
(16) Olson, R. J.; Shalapyonok, A.; Kalb, D. J.; Graves, S. W.; Sosik, H. M. Imaging FlowCytobot Modified for High Throughput by In-Line Acoustic Focusing of Sample Particles. *Limnol. Oceanogr.: Methods* **2017**, *15* (10), 867−874.
(17) Göröcs, Z.; Tamamitsu, M.; Bianco, V.; Wolf, P.; Roy, S.; Shindo, K.; Yanny, K.; Wu, Y.; Koydemir, H. C.; Rivenson, Y.; Ozcan, A. A Deep Learning-Enabled Portable Imaging Flow Cytometer for Cost-Effective, High-Throughput, and Label-Free Analysis of Natural Water Samples. *Light: Sci. Appl.* **2018**, *7* (1), 66.
(18) Göröcs, Z.; Baum, D.; Song, F.; de Haan, K.; Koydemir, H. C.; Qiu, Y.; Cai, Z.; Skandakumar, T.; Peterman, S.; Tamamitsu, M.; Ozcan, A. Label-Free Detection of Giardia Lamblia Cysts Using a Deep Learning-Enabled Portable Imaging Flow Cytometer. *Lab. Chip* **2020**, na.
(19) Isikman, S. O.; Greenbaum, A.; Luo, W.; Coskun, A. F.; Ozcan, A. Giga-Pixel Lensfree Holographic Microscopy and Tomography Using Color Image Sensors. *PLoS One* **2012**, *7* (9), No. e45044.
(20) Zhang, Y.; Wang, H.; Wu, Y.; Tamamitsu, M.; Ozcan, A. Edge Sparsity Criterion for Robust Holographic Autofocusing. *Opt. Lett.* **2017**, *42* (19), 3824−3827.
(21) Greenbaum, A.; Luo, W.; Su, T.-W.; Göröcs, Z.; Xue, L.; Isikman, S. O.; Coskun, A. F.; Mudanyali, O.; Ozcan, A. Imaging without Lenses: Achievements and Remaining Challenges of Wide-Field on-Chip Microscopy. *Nat. Methods* **2012**, *9* (9), 889−895.
(22) Bishara, W.; Su, T.-W.; Coskun, A. F.; Ozcan, A. Lensfree On-Chip Microscopy over a Wide Field-of-View Using Pixel Super-Resolution. *Opt. Express* **2010**, *18* (11), 11181−11191.
(23) NCMA at Bigelow Laboratory, https://ncma.bigelow.org/ (accessed Sep 8, 2020).
(24) Gonzalez, R. C. *Digital Image Processing*; Pearson Education, 2009.
(25) Soille, P. *Morphological Image Analysis: Principles and Applications*, 2nd ed.; Springer-Verlag: Berlin, Heidelberg, 2004, DOI: 10.1007/978-3-662-05088-0.
(26) MATLAB - MathWorks, https://www.mathworks.com/products/matlab.html (accessed Oct 2, 2020).
(27) Bottema, M. J. Circularity of Objects in Images. *2000 IEEE International Conference on Acoustics, Speech, and Signal Processing. Proceedings (Cat. No.00CH37100)*; IEEE, 2000; Vol. 4, pp 2247−2250, DOI: 10.1109/ICASSP.2000.859286.
(28) Kullback, S.; Leibler, R. A. On Information and Sufficiency. *Ann. Math. Stat.* **1951**, *22* (1), 79−86.
(29) Jeffreys, H. An Invariant Form for the Prior Probability in Estimation Problems. *Proc. R. Soc. London Ser. Math. Phys. Sci.* **1946**, *186* (1007), 453−461.
(30) Huang, G.; Liu, Z.; van der Maaten, L.; Weinberger, K. Q. Densely Connected Convolutional Networks. *arXiv:1608.06993 [cs.CV]* **2018**, na.
(31) Hemocytometer vs Automated Cell Counter - Which to Buy? | Bio-Rad, https://www.bio-rad.com/featured/en/hemocytometer.html (accessed Sep 4, 2020).
(32) Kaeberlein, T.; Lewis, K.; Epstein, S. S. Isolating "Uncultivable" Microorganisms in Pure Culture in a Simulated Natural Environment. *Science* **2002**, *296* (5570), 1127−1129.

https://dx.doi.org/10.1021/acsphotonics.1c00220
ACS Photonics XXXX, XXX, XXX−XXX

Supplementary information for

Phenotypic analysis of microalgae populations using label-free imaging flow cytometry and deep learning

Çağatay Işıl[1,2,3,†], Kevin de Haan[1,2,3,†], Zoltán Görücs[1,2,3,†], Hatice Ceylan Koydemir[1,2,3,†], Spencer Peterman[2], David Baum[1], Fang Song[1], Thamira Skandakumar[2], Esin Gumustekin[4], and Aydogan Ozcan[1,2,3,*]

[1]*Electrical and Computer Engineering Department, University of California, Los Angeles, CA, 90095, USA*

[2]*Bioengineering Department, University of California, Los Angeles, CA, 90095, USA*

[3]*California NanoSystems Institute (CNSI), University of California, Los Angeles, CA, 90095, USA*

[4]*Neuroscience Department, University of California, Los Angeles, CA, 90095, USA*

*ozcan@ucla.edu

Email addresses:

Çağatay Işıl: cagatayisil@ucla.edu
Kevin de Haan: kdehaan@ucla.edu
Zoltán Görücs: zoligorocs@g.ucla.edu
Hatice Ceylan Koydemir: hceylan@ucla.edu
Spencer Peterman: speterman98@gmail.com
David Baum: davidandrewbaum@gmail.com
Fang Song: fangsong@ucla.edu
Thamira Skandakumar: skandakumar.thamira@gmail.com
Esin Gumustekin: egumustekin@ucla.edu
Aydogan Ozcan: ozcan@ucla.edu

†Authors contributed equally
*Corresponding author: Aydogan Ozcan
420 Westwood Plaza
Engineering IV. 68-119
Los Angeles, CA 90095
USA
Tel.: +1(310)825-0915
Fax: +1(310)206-4883
Email: ozcan@ucla.edu

1. Supplementary Figures

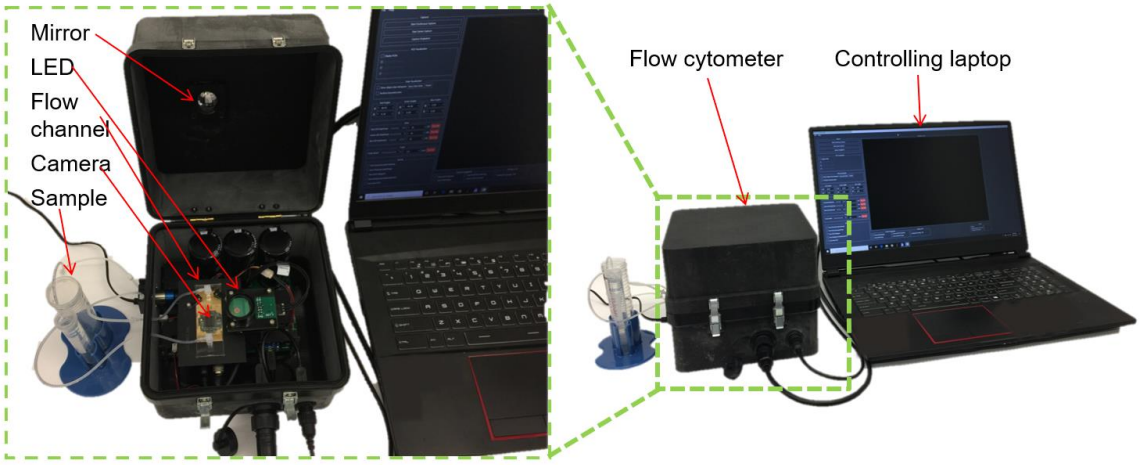

Figure S1. Holographic imaging flow cytometer. The imaging flow cytometer automatically analyzes the algae within water samples at a throughput of 100 mL/h. A laptop is used for system control and data processing. Inset shows the main components of the system.

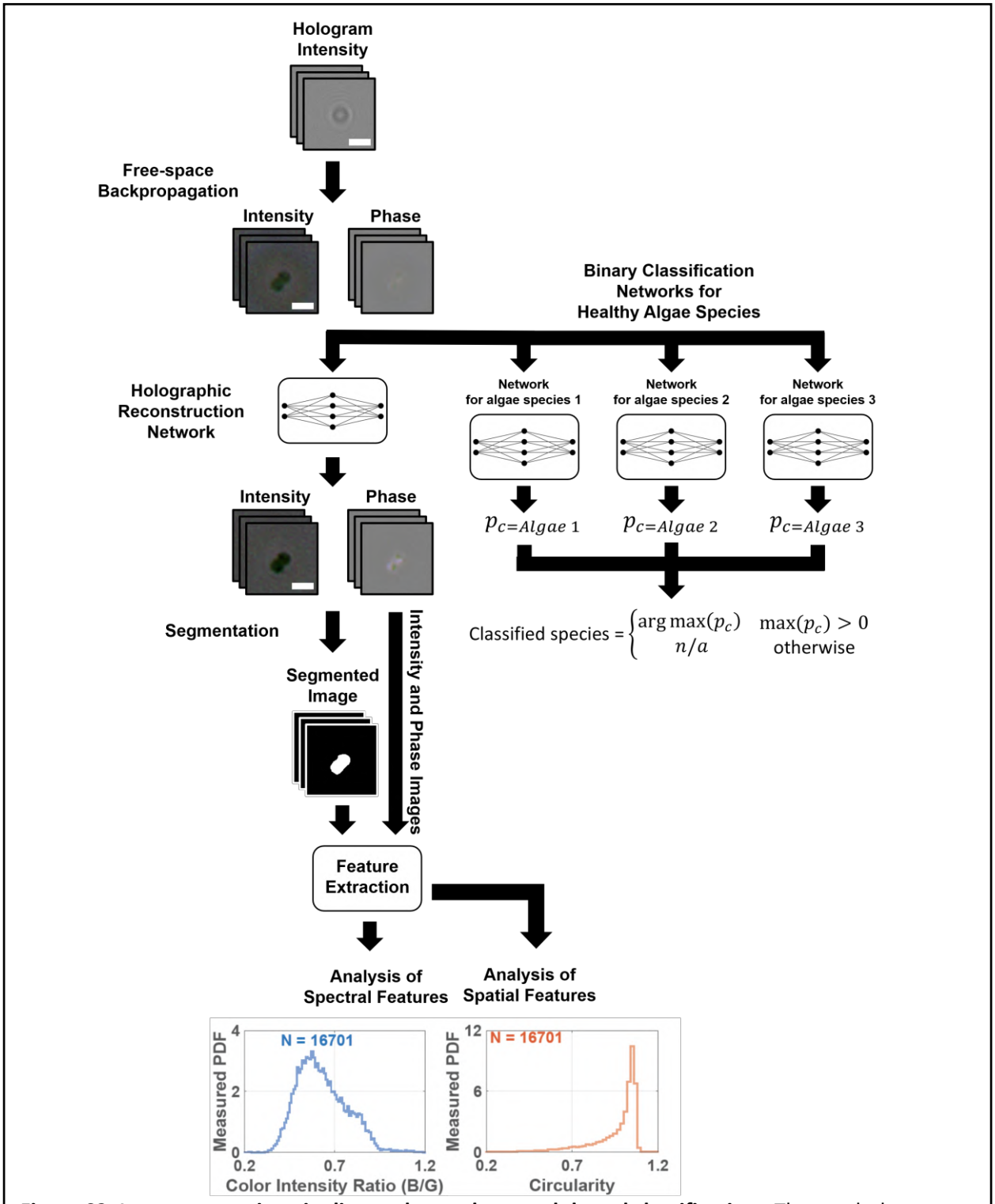

Figure S2. Image processing pipeline and neural network-based classification. The raw holograms pass through a multi-step image processing procedure which first backpropagates and removes twin image artifacts on both the phase and intensity images. Using these reconstructed images, features are extracted to perform statistical analyses. Images that have been backpropagated are used to classify the algae species. Scale bars: 20 µm.

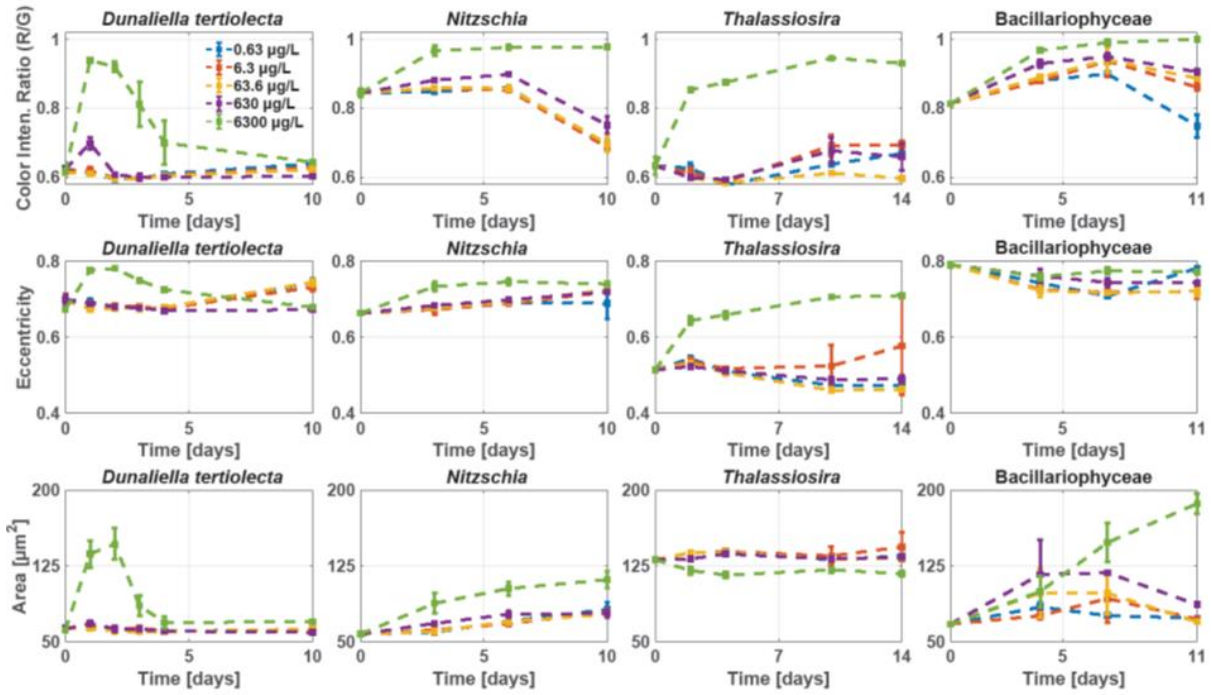

Figure S3 - Effects of copper exposure on four different algae monocultures monitored over time using the holographic imaging flow cytometer. Various concentrations of copper are introduced to the algae monocultures at day 0, and the samples are measured at regular time intervals using the imaging flow cytometer. The device analyses ~5000-15000 individual algae images per measurement. Three of the monitored features - color intensity ratio (Red/Green), eccentricity, and area - are displayed here to visualize the effect of various copper concentrations over time. The median values of the measured PDFs of the corresponding features for each day as well as the copper concentration are shown. Error bars indicate the standard deviation across repeated experiments.

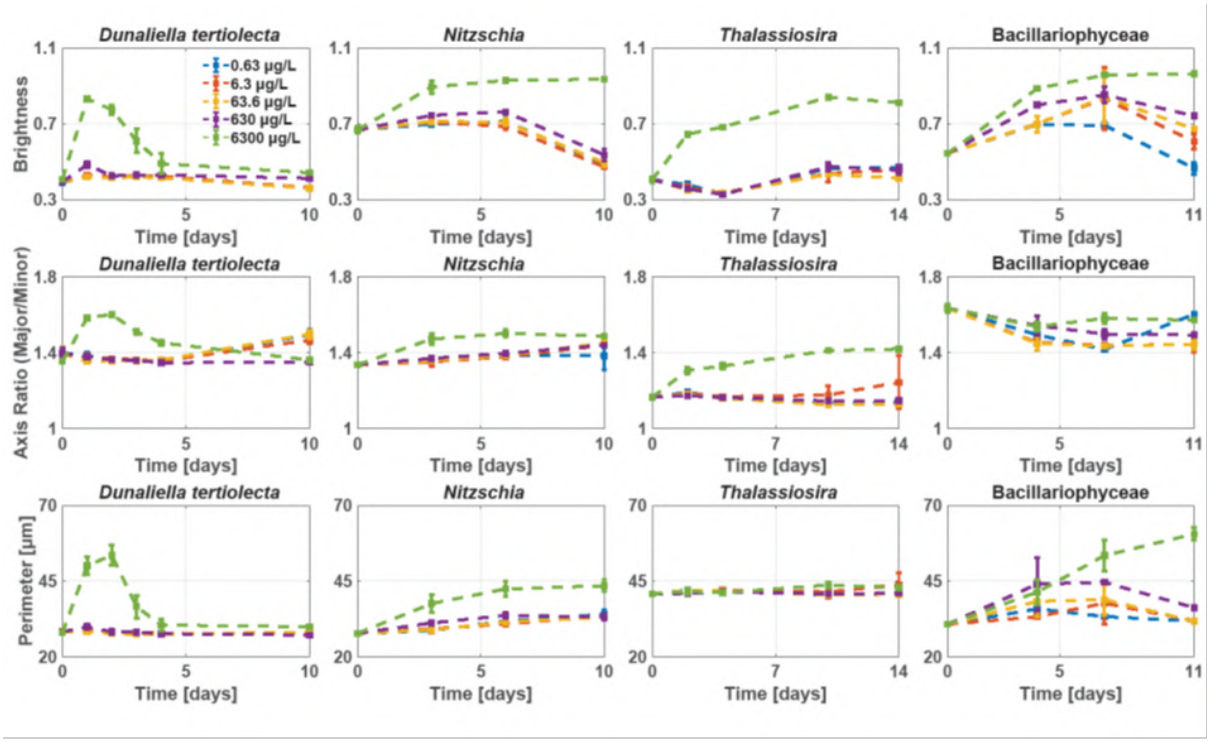

Figure S4 - Effects of copper exposure on four different algae monocultures monitored over time using the holographic imaging flow cytometer. Various concentrations of copper are introduced to the algae monocultures at day 0, and the samples are measured at regular time intervals by the imaging flow cytometer. The device analyses ~5000-15000 individual algae images per measurement. Plots of three of the monitored features- brightness, axis ratio, and perimeter- are used to visualize the effect of various copper concentrations over time. The median values of the measured PDFs of the corresponding features for each day as well as the copper concentration are shown. Error bars indicate the standard deviation across repeated experiments.

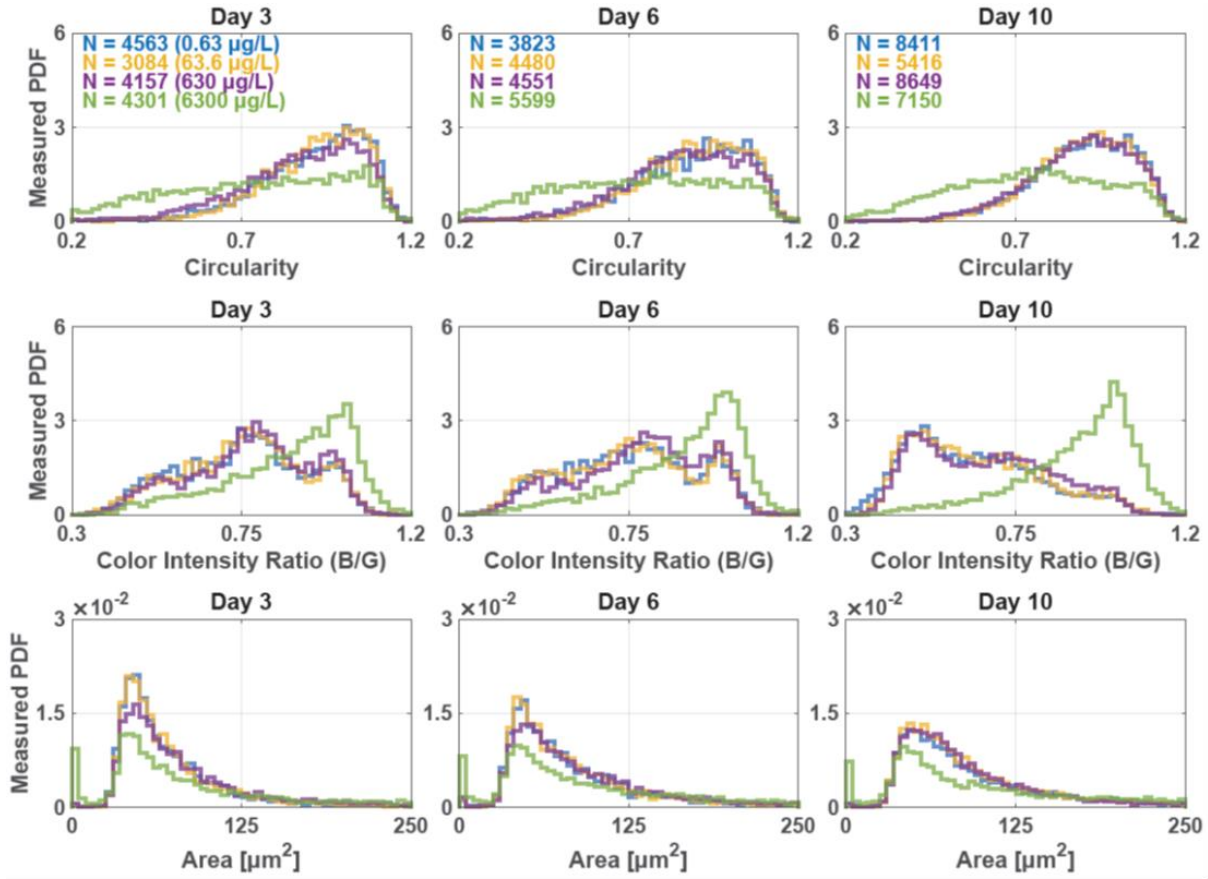

Figure S5 - Normalized histograms (measured PDFs) of color intensity ratio, circularity, and area of algae at different copper concentrations for *Nitzschia*.

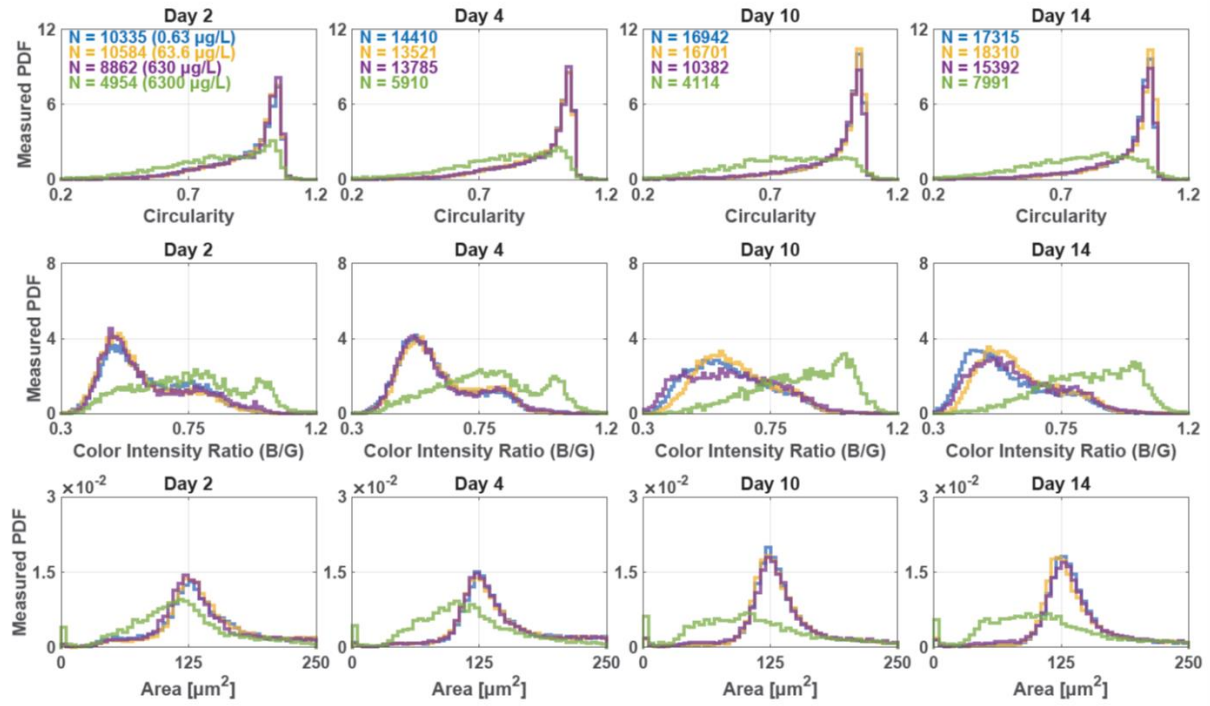

Figure S6 - Normalized histograms (measured PDFs) of color intensity ratio, circularity, and area of the algae at different copper concentrations for *Thalassiosira*.

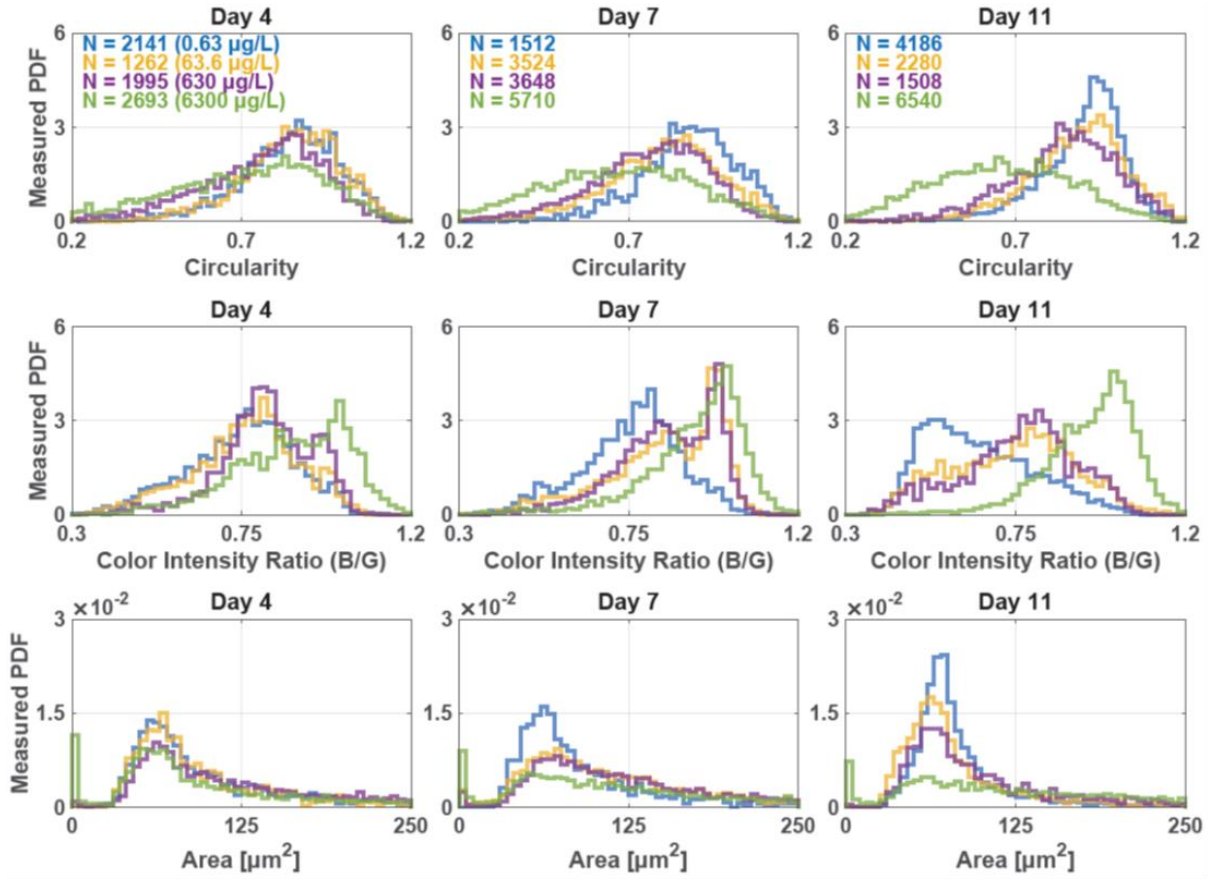

Figure S7 - Normalized histograms (measured PDFs) of color intensity ratio, circularity, and area of algae at different copper concentrations for Bacillariophyceae.

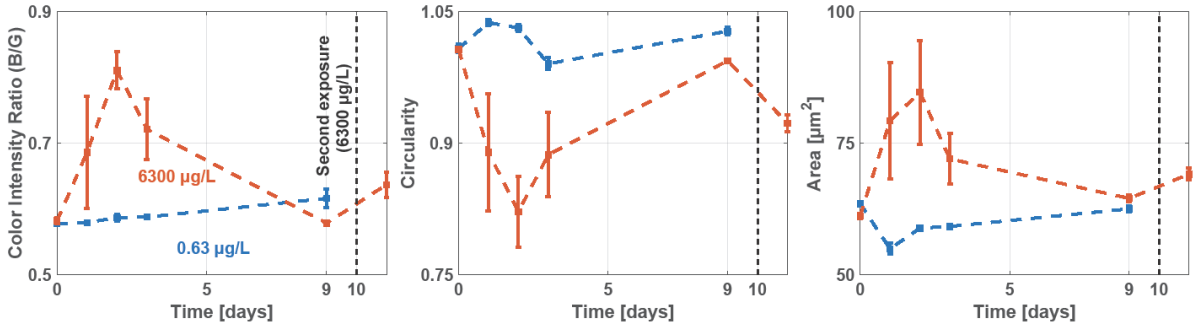

Figure S8 - Effects of multiple copper exposure on *Dunaliella tertiolecta*. Three different features are compared as a function of time at two different copper concentrations. The algae are exposed to copper for a second time on day 10.

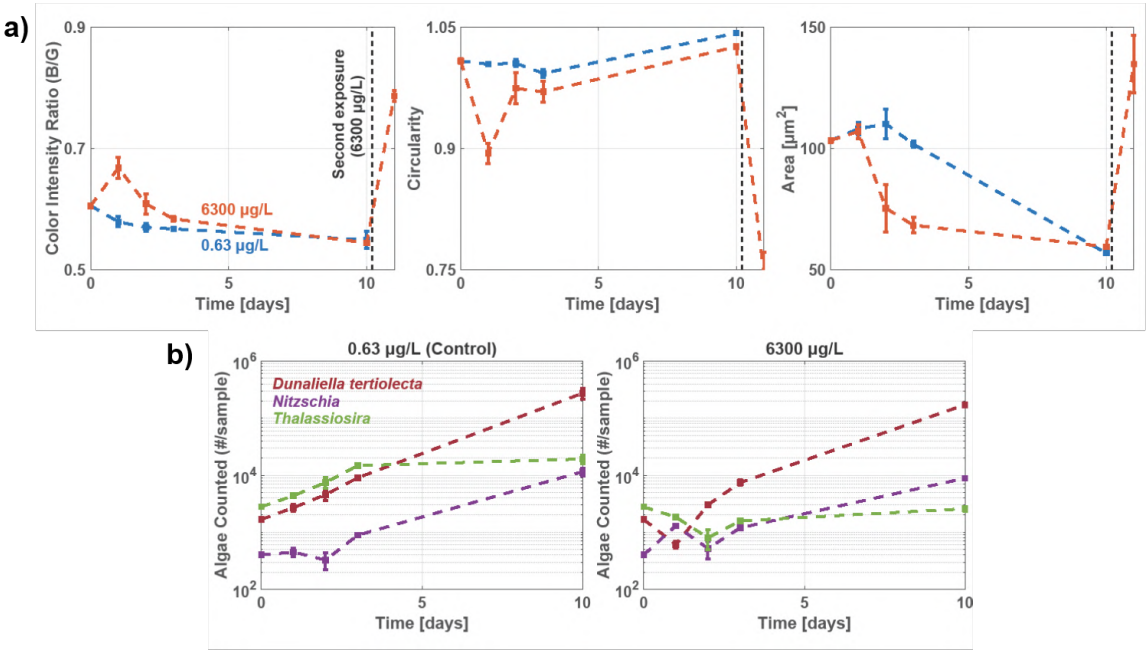

Figure S9 - Effects of multiple copper exposure on an algae mixture containing *Dunaliella tertiolecta, Nitzschia*, and *Thalassiosira*. a) A comparison of different features at different copper concentrations over time is shown for the algae mixture. The median values of the measured features are plotted. The error bars indicate the standard deviation across repeated experiments. b) Estimated average number of algae from each species within the sample.

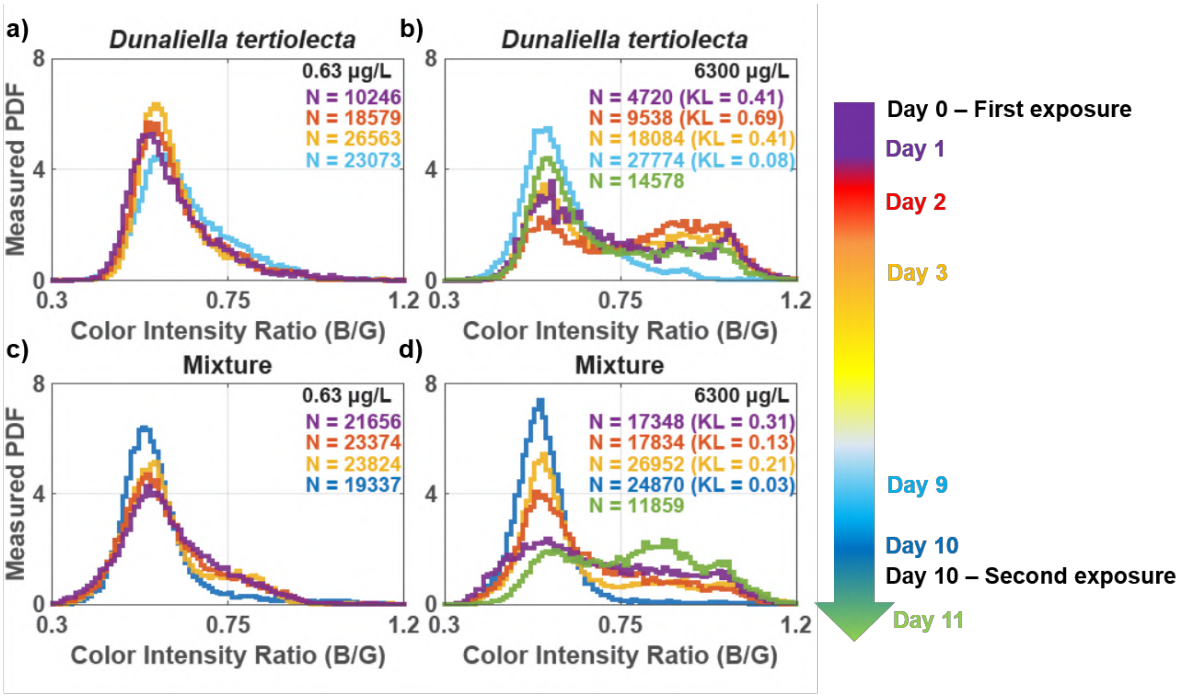

Figure S10 - Effects of multiple copper exposure on the PDFs of color intensity ratio feature for *Dunaliella tertiolecta* and an algae mixture (*Dunaliella tertiolecta, Nitzschia, Thalassiosira*). a) and b) show PDFs of the B/G color intensity ratio for *Dunaliella tertiolecta* grown at the control concentration (0.63 µg/L) and the highest concentration (6300 µg/L), respectively. c) and d) show PDFs of the B/G color intensity ratio for the mixture (containing *Dunaliella tertiolecta*, *Nitzschia*, *Thalassiosira*) grown at the control concentration (0.63 µg/L) and the highest concentration (6300 µg/L), respectively.

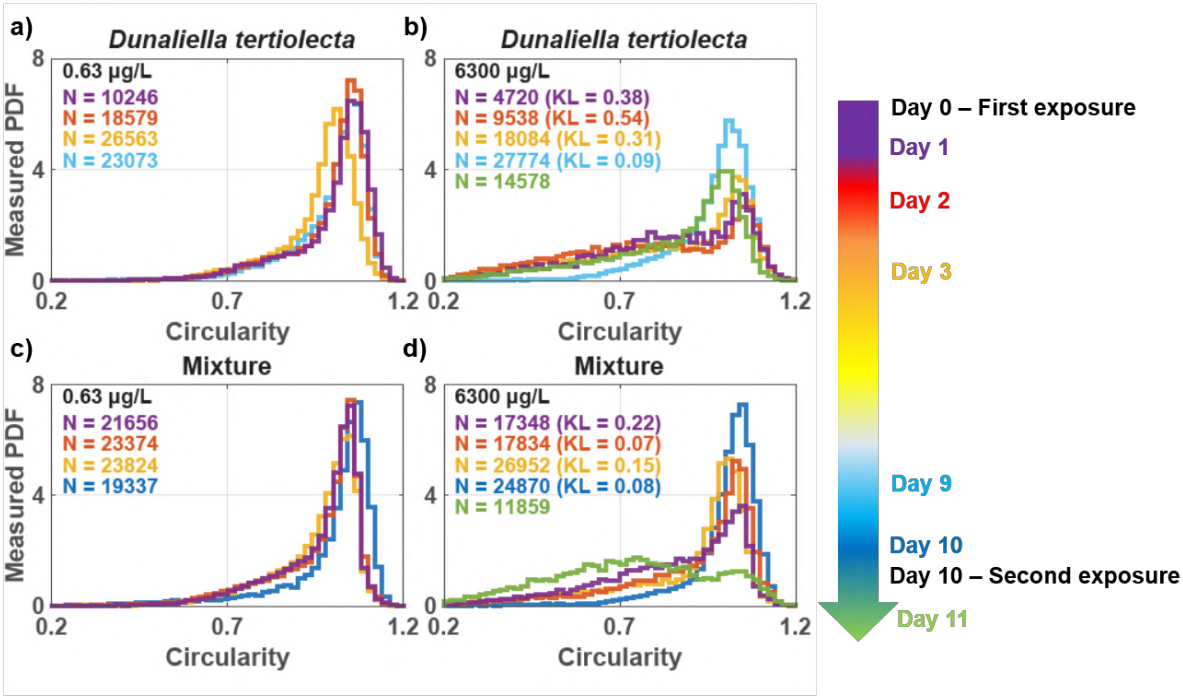

Figure S11 - Effects of multiple copper exposure over time on the PDFs of circularity feature for *Dunaliella tertiolecta* and an algae mixture (*Dunaliella tertiolecta, Nitzschia, Thalassiosira*). a) and b) show PDFs of the circularity of *Dunaliella tertiolecta* grown at the control concentration (0.63 µg/L) and the highest concentration (6300 µg/L), respectively. c) and d) show PDFs of the circularity of the mixture (containing *Dunaliella tertiolecta*, *Nitzschia*, *Thalassiosira*) grown at the control concentration (0.63 µg/L) and the highest concentration (6300 µg/L), respectively.

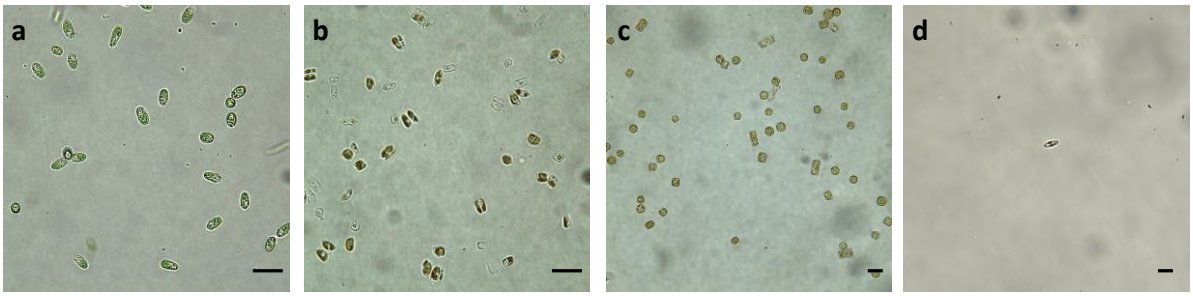

Figure S12 - Images of studied algae species captured using a regular brightfield microscope. a) *D. tertiolecta* (CCMP1320) (40x – 0.95 NA), b) *Nitzschia* (CCMP1698) (40x – 0.95 NA), c) *Thalassiosira* (CCMP2929) (40x – 0.95 NA), and d) Bacillariophyceae (CCMP2024) (20x – 0.75 NA). Scale bar is 20 µm.

2. Supplementary Table

Table S1. The algae species used in our experiments and their properties[1].

	CCMP1320 *Dunaliella tertiolecta*	**CCMP2929** *Thalassiosira sp.*	**CCMP1698** *Nitzschia sp.*	**CCMP2024** Bacillariophyceae
Growth media	L1	L1	L1	L1
Known temperature range	11 - 28°C	22 - 26°C	22-26°C	22 - 26°C
Cell length (min)	6	10	6	27
Cell length (max)	9	14	30	30
Cell width (min)	0	9	3	5
Cell width (max)	0	14	6	7

Reference

(1) NCMA at Bigelow Laboratory https://ncma.bigelow.org/ (accessed Sep 8, 2020).